ACS APPLIED MATERIALS & INTERFACES

Research Article

www.acsami.org

Improving Liquid-Crystal-Based Biosensing in Aqueous Phases

Wilder Iglesias,[†] Nicholas L. Abbott,[‡] Elizabeth K. Mann,[§] and Antal Jákli*[,†,∇]

[†]Liquid Crystal Institute, Kent State University, Kent, Ohio 44242, United States

[‡]Chemical and Biological Engineering, University of Wisconsin−Madison, Madison, Wisconsin 53706, United States

[§]Physics Department, Kent State University, Kent, Ohio 44242, United States

[∇]Institute for Solid State Physics and Optics, Wigner Research Centre for Physics, Hungarian Academy of Sciences, P.O. Box. 49, H-1525 Budapest, Hungary

ABSTRACT: Liquid crystal (LC)-based biological sensors permit the study of aqueous biological samples without the need for the labeling of biological species with fluorescent dyes (which can be laborious and change the properties of the biological sample under study). To date, studies of LC-based biosensors have explored only a narrow range of the liquid crystal/alignment layer combinations essential to their operation. Here, we report a study of the role of LC elastic constants and the surface anchoring energy in determining the sensitivity of LC-based biosensors. By investigating a mixture of rod-shape and bent-shape mesogens, and three different alignment layers, we were able to widen the useful detection range of a LC-based sensor by providing an almost-linear mapping of effective birefringence with anionic surfactant concentrations between 0.05 mM and 1 mM (model target analyte). These studies pave the way for optimization of LC-based biosensors and reveal the importance of the choice of both the LC material and the alignment layer in determining sensor properties.

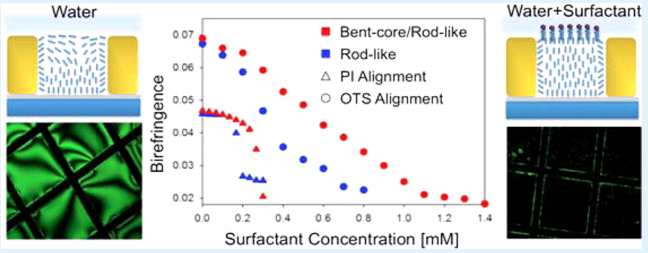

KEYWORDS: *biosensing, anchoring energy, surfaces, liquid crystals, bent-core molecules, elastic constants*

I. INTRODUCTION

Studies of interfacial phenomena involving liquid crystals (LCs) near solid surfaces have been pivotal in the development of a range of electro-optical devices (including LC displays).[1−3] Surface science tools have yielded important details regarding molecular level interactions that couple the structure of the solid surface to the ordering of mesogens at the interface, which, in turn, transfer their organizational information to the bulk LC via long-range orientational order of the LC. The sensitivity of LCs to surface properties is also the basis of a more-recent series of studies of interfaces formed between LCs and immiscible aqueous phases. A remarkably diverse range of ordering transitions occurs as amphiphilic molecules (surfactants and lipids), polymers, or proteins assemble at interfaces between LCs and aqueous phases. The interfacial phenomena can be monitored using the macroscopic alignment of the LC director as an imaging tool for sensing key molecular and nanoscopic events at the LC/biomaterial-laden interface.[4−9]

An experimental setup that has been widely used for LC-based sensing of biological samples in water is shown in Figure 1. It involves an interface between an aqueous phase and a water-immiscible thermotropic LC in its nematic phase. Most studies to date have used the LC 4′-pentyl-4-cyanobiphenyl (5CB) at room temperature. The LC is placed in the holes of a gold transmission electron microscopy (TEM) grid that is supported on a glass microscope slide treated with different homeotropic alignment layers,[9] most often octadecyltrichlorosilane (OTS). Immersion of this simple setup into an aqueous phase leads to the formation of a stable interface between the aqueous phase and the LC.

By performing the study reported in this paper, we aimed to advance current biosensing techniques based on LCs by manipulating the bulk elastic constants and surface anchoring properties of the surface/mesogen combinations. The bulk elastic properties are determined by K_1, K_2, and K_3, which are "elastic constants" that dictate the changes in the Frank free energy per unit volume F_d, when the nematic liquid crystal is splayed, twisted, or bent, respectively:[10]

$$F_d = \frac{1}{2}K_1(\vec{\nabla}\cdot\vec{n})^2 + \frac{1}{2}K_2(\vec{n}\cdot\vec{\nabla}\times\vec{n})^2 + \frac{1}{2}K_3(\vec{n}\times\vec{\nabla}\times\vec{n})^2 \quad (1)$$

where $\vec{n}$ is the LC director. These constants are unique and characteristic of the hundreds of thousands of different LC materials synthesized and characterized to date. The director distortion in the bulk transfers a torque to the surfaces of the LC, and the equilibrium bulk configuration is determined by the torque balance at the surfaces. The surface interactions can be approximated by the Rapini−Papoular expression[11] for the energy per unit area:

$$\Phi_s^{\pm} = \frac{1}{2}W^{\pm}\sin^2(\theta^{\pm} - \theta_e^{\pm}) \quad (2)$$

Received: September 18, 2012
Accepted: November 16, 2012
Published: November 16, 2012

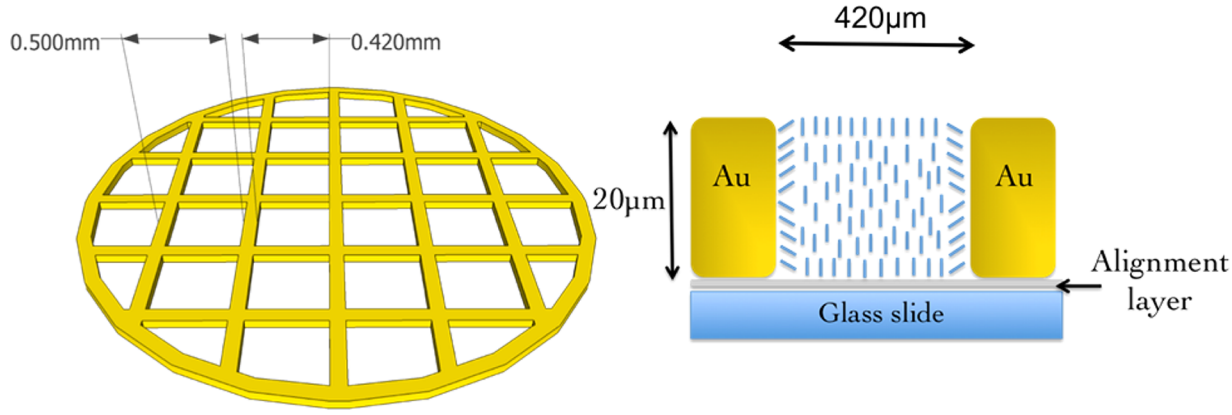

Figure 1. Schematic illustration of the experimental system used to study the adsorption of amphiphiles at the aqueous/liquid crystal interfaces. TEM gold grids (50 lines/in. square mesh) obtained from Electron Microscopy Sciences.

where $W^{\pm} > 0$ are the anchoring strengths at the different surfaces and $\theta_e^{\pm}$ are the surface easy tilt angles, i.e., the directions imposed by external surface conditions.

An additional key concept used to describe the anchoring of LCs at surfaces is the extrapolation length. The extrapolation length $b = K/W$ can be related to the distance from the surface where θ would reach the easy axis value without disturbing the $d\theta/dz$ = constant dependence valid in the bulk (see Figure 2).

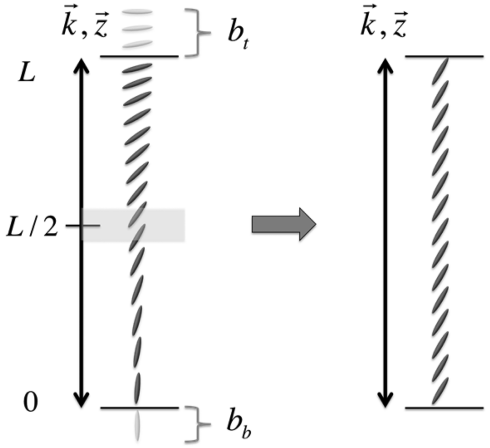

Figure 2. LC director profile sketch in a cell of thickness L. (Left) Hybrid configuration with different anchoring energies at the surfaces. (Right) Equivalent LC cell with a uniform director angle through the z-direction, based on the hybrid cell director angle at the $L/2$ position.

When $b \ll L$ (strong anchoring), the bulk elastic properties govern the director profile, whereas when $b/L \approx 1$ (weak anchoring), the alignment surfaces will also play an important role.

In this paper, we advance the use of LCs for biosensing by identifying new LC materials and alignment methods that provide a wider sensing range for a surfactant (used as a model analyte). We note that sensing-range linearity is generally a highly desired attribute of a biosensor. We also note that, although past studies have generally interpreted the orientational response of LCs to adsorbates at aqueous/LC interfaces as resulting from changes in the easy axis of the LCs,[4−9] in this paper, we offer an interpretation of our experimental results in terms of a reduction in the anchoring energy (without a change in the easy axis). We conclude that a complete description of the operation of LC-based sensors will likely need to include consideration of both changes in the easy axis and anchoring energies of LCs, as induced by targeted analytes. Overall, the results reported in this paper enable new approaches for investigations of the self-assembly of molecules at interfaces, as well as opportunities for technological advances in areas such as chemical and biological sensing and the design of stimuli-responsive materials.

II. MATERIALS AND METHODS

II.1. Alignment Layers. In addition to the previously tested OTS-treated glass, two other homeotropic alignment surfaces—polyimide (PI) and a bent-core layer of amphiphilic molecules (Z4)—were used to probe the role played by the anchoring energy of the bottom surface. All these alignment layers were deposited on glass slides cleaned in water by using an ultrasonic cleaner (Branson B200), and washed with a solution of isopropanol/water and placed immediately in an oven at 80 °C for 15 min. For the OTS coating, the clean glass slides were immersed in an OTS/heptane solution at 0.5 mM for 30 min, rinsed with dichloromethane (DCM or methylene chloride) three times and dried with nitrogen. For the PI coating, a drop of Nissan SE-1211 was placed in the center of the glass slide and spin-coated for 20 s at 2500 rpm. Next, this slide was soft-baked for 1−2 min at 90 °C on a hot plate and then hard-baked in an oven for 1 h at 108 °C. For the bent-core surface layer, a monolayer of the banana-shaped LC molecules, Z4[12] (shown in Figure 3), spread on water in a Langmuir

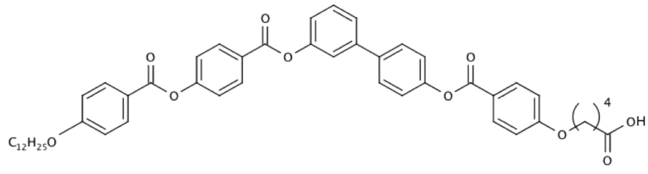

Figure 3. Amphiphilic bent-core molecule with four carbons between the carboxylic headgroup and aromatic core. The molecule was used as a successful homeotropic alignment layer for 5CB in ref 13.

trough was transferred to a clean glass slide using the inverse Langmuir/Schaefer deposition. To achieve homeotropic alignment, the material is deposited at high surface pressure (~30 mN/m), as described in earlier papers.[13]

II.2. Gold Grids. The alignment-layer-coated glass slides were used to form the base of optical cells. Gold-coated TEM grids (obtained from Electron Microscopy Sciences; see Figure

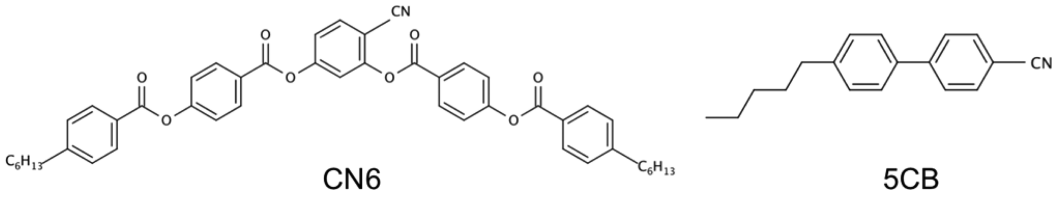

Figure 4. Chemical structures of mesogens used in this work. (Left) A nitrile-substituted nematic bent-core liquid crystal (CN6). (Right) A standard rodlike liquid crystal (5CB) that forms a nematic phase at room temperature.

1) were placed onto the coated glass slides. Square gold-coated meshes with 50 and 75 lines/in. were tested, giving similar results; the former one was chosen, since the edge effects are less important for larger hole sizes.[14] Grids were used more than once and stored in ethanol. Before each use, they were washed by rinsing three times with ethanol, three times with methanol, and three times with either chloroform or dichloromethane.

II.3. LC Mesogens. Bent-core liquid crystal molecules (BCLC) have been shown[15] to possess distinctively lower bend elastic constants due their favorable molecular shape for bend distortions. This lower bend elastic constant makes BCLC interesting candidates for biosensing. On the other hand, the banana shape promotes molecular locking into layers that favor smectic structures. Although a nematic phase of BCLCs can be achieved by frustrating this locking mechanism by bulky substitutions in the central ring of a bent-shape molecule, the nematic phase usually occurs at high temperatures where thermal fluctuations are sufficient to break the locking. This presents a challenge for biosensors, which require a LC material with a nematic phase between room temperature and 37 °C. Fortunately, the nematic phase range of BCLCs can be lowered by mixing them with calamitic mesogens,[16] where the calamitic mesogens frustrate the locking of the bent cores and the thermal energy necessary to induce a nematic phase is smaller.

To achieve the appropriate temperature range and low elastic constants, mixtures of a bent-core mesogen with a CN substitution (CN6)[17] with the well-known 5CB (see molecular structures in Figure 4) were studied. Since in a nematic phase the elastic constant values diminish as we approach the Iso-N transition temperature,[18] we aimed to find a mixture of these two components such that the isotropic−nematic transition was close to the working temperatures, and the concentration of bent-shaped liquid crystal was large enough to lower the elastic constants of the blend.

Table 1 shows that a blend of 5CB/CN6 at 57/43 (based on wt %) was a good candidate for our study, since the nematic−isotropic phase transition temperature is similar to that of 5CB and the concentration of the bent-core mesogen is sufficiently high to lower the elastic constant of the blend.

Table 1. Concentration Dependence of the N−Iso and Iso−N Transitions[a] of 5CB/CN6 Mixtures

5CB (wt %)	CN6 (wt %)	N−Iso heating (°C)	Iso−N cooling (°C)
100	0	35.5	35.2
65	35	36.4	35.8
57	43	38.8	37.9
34	66	45.1	41.9
0	100	101	98

[a]Iso = isotropic fluid, N = nematic phase.

III. MEASUREMENTS

III.1. Elastic Constants. To find the Frank elastic constants, the Freedericksz transitions were measured in magnetic and electric fields, following the procedure described in ref 15. Thick (d = 22 μm) homogeneously aligned (planar) films of 5CB and CN6/5CB were placed in a temperature-regulated oven mounted between the pole faces of a large electromagnet in orientations shown in Figure 5. One direction of the

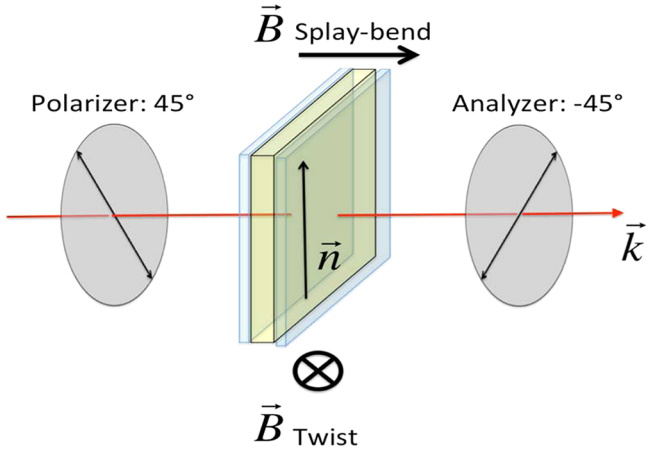

Figure 5. Schematic illustrations for the Freedericksz transition measurements.

magnetic field corresponds to a field-induced splay-bend deformation, and the other one corresponds to a pure twist distortion. A 4-mW HeNe laser, normally incident on the sample, together with a polarizer−analyzer combination and an amplified photodetector (Thorlabs, Model PDA55), were used to detect optically the threshold field B_t for the onset of the director deformations. The magnetic field, monitored with a small Hall probe mounted near the sample, could be varied continuously from 0 to 1.3T, and was highly uniform over the sample cell volume. In addition to the optical transmission data, the cell capacitance was also recorded as a function of the applied magnetic field using a precision capacitance bridge (Andeen−Hagerling, Model 2500A) with a probe voltage of 0.1 V at a frequency of 1 kHz. Finally, the change of B_t, as a function of an AC voltage ranging from 0 to 2 V_{rms} at 1 kHz, was determined using the optical transmission method in the splay-bend configuration.[15]

The measurements were analyzed by equations valid for aligned uniaxial nematics;[19] the elastic constants determined in this way are shown in Table 2. The results obtained for 5CB at 24 °C are in good agreement with values published in the literature.[20−23] It can be seen that all three elastic constants are smaller for the mixture than for pure 5CB.

III.2. Surface Anchoring Energy. There are several methods of determining the anchoring strength (energy per

dx.doi.org/10.1021/am301952f | ACS Appl. Mater. Interfaces 2012, 4, 6884−6890

Table 2. Elastic Constant Results for 5CB and Mixtures of 5CB/CN6 at 57/43 wt % Measured at 24 and 30 °C

parameter	5CB at 24 °C	5CB at 30 °C	5CB/CN6 at 24 °C	5CB/CN6 at 30 °C
K_1 (pN)	6.5	5.3	5.5	4.9
K_2 (pN)	3.5	3.2	2.9	2.7
K_3 (pN)	9.8	5.8	8.3	5.6

unit area), most directly by finding the voltage necessary to overcome the preferred orientation of LC molecules at the surface. Below this voltage, the director will relax quickly (within several milliseconds) after the field has turned off. Above the anchoring threshold, however, the relaxation is gradual (requiring several seconds or minutes), as dictated by a surface nucleation process, whereby the mesogens adsorbed at the surface return to their original orientations. The threshold voltage to break the anchoring can be related to the surface anchoring energy per unit area W_0, by equating it with the dielectric energy density $^1/_2\Delta\varepsilon E^2$ ($\Delta\varepsilon$ is the dielectric anisotropy, $E = V/d$ is the electric field, and V is the voltage applied across the electrodes separated by a distance d), multiplied by the electric coherence length,[24] $\xi_3 = 1/E(K_3/\Delta\varepsilon)$, such that

$$W_0 = \frac{V}{2d}\sqrt{\Delta\varepsilon K_3} \tag{3}$$

Since the materials that we studied have positive dielectric anisotropies, we used an in-plane switching (IPS) liquid crystal cell with homeotropic substrates. It was found that the anchoring for the Nissan SE-1211 PI breaks at $V \approx 107$ V for 5CB and ~93 V for 5CB/CN6 with a $d = 20$ μm gap between electrodes. These provide values of $W_0 \approx 1.4 \times 10^{-4}$ J/m^2 for 5CB and $W_0 \approx 0.9 \times 10^{-4}$ J/m^2 for the 5CB/6CN, respectively. The anchoring energy measurements for 5CB coincide with those published in the literature.[25−27]

III.3. Polarizing Optical Microscopy (POM). The TEM grid filled with the LC material, supported on a homeotropic alignment layer, is dark in POM between crossed polarizers (viewed in air), because the LC film adopts a homeotropic orientation at the interface with air (see left column of Figure 6). Immersion of the sample in deionized water results in a hybrid alignment, since the water promotes planar alignment at the top interface of the LC, while the bottom surface is homeotropic. This hybrid alignment leads to a LC samples that exhibits a bright appearance and a typical defect structure (see second column in Figure 6). When a surfactant, sodium dodecyl sulfate (SDS), is added to the water, the adsorbed layer reduces the effective birefringence, due to the interaction of the SDS with the LC interface (third column in Figure 6). As described by Lockwood et al.,[6,8] the pretilt angle at the top surface continuously increases with surfactant concentration until homeotropic alignment is achieved. To calculate the effective birefringence (Δn_{eff}) of the LC film, we measured the transmitted intensity of light (I), under monochromatic (λ = 550 nm) illumination with the optical axis of the sample positioned 45° from the two crossed polarizers, and determined an effective refractive index contrast Δn_{eff} using eq 4, which is exactly valid with $\Delta n_{\text{eff}} = \Delta n$ for a uniform cell:

$$I = I_0 \sin^2\left[\pi\Delta n_{\text{eff}}\left(\frac{d}{\lambda}\right)\right] \tag{4}$$

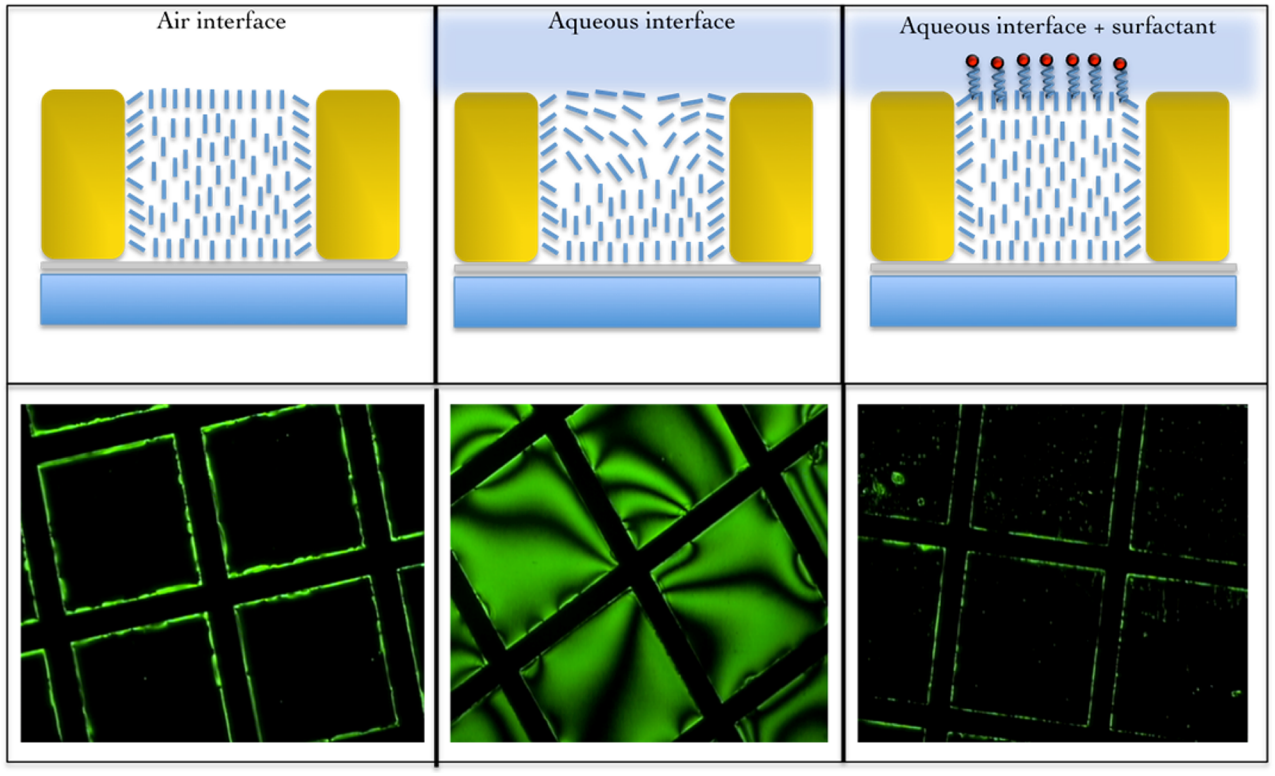

Figure 6. LC at aqueous interfaces. (Top) Schematic illustration of the nematic director in the TEM grid. (Bottom) Texture captured by POM of the illustration above. (First column) LC at the air interface. (Second column) LC at the pure water interface. (Third column) LC at the water interface with a high concentration of surfactant.

dx.doi.org/10.1021/am301952f | ACS Appl. Mater. Interfaces 2012, 4, 6884−6890

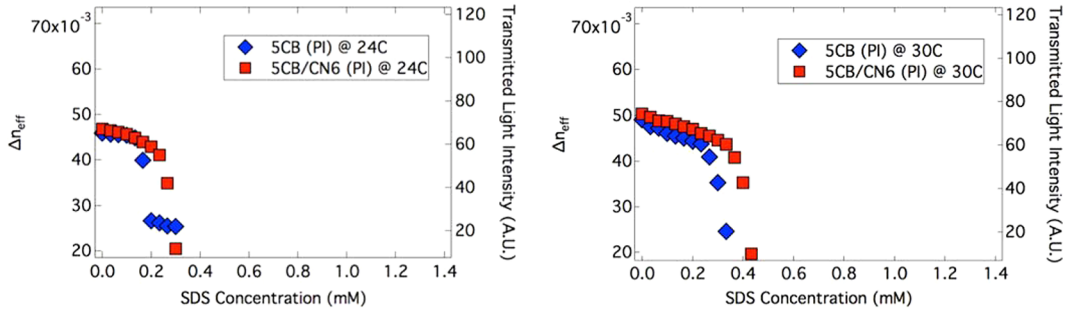

Figure 7. Birefringence and transmitted light for two different nematic liquid crystals, 5CB and the 5CB/CN6 mixture discussed in the text, versus surfactant concentration using the PI alignment layer. (Left) SDS sensing at 24 °C; (right) SDS sensing at 30 °C.

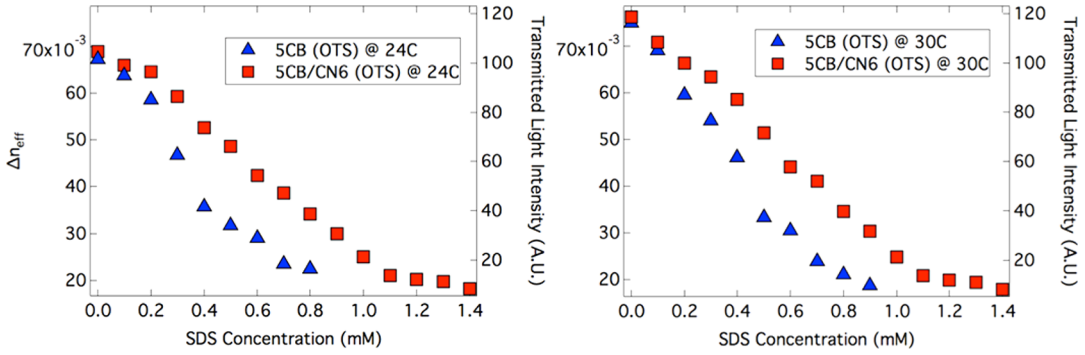

Figure 8. Birefringence and transmitted light for two different nematic liquid crystals, 5CB and the 5CB/CN6 mixture discussed in the text, versus surfactant concentration, using OTS as the alignment layer. (Left) SDS sensing at 24 °C; (right) SDS sensing at 30 °C.

where I_0 is the incoming light intensity and d is the thickness of the LC cell (d = 22 μm). I_0 can be found by measuring I when the LC is under pure water and the bottom alignment layer also produces a planar alignment. For this configuration, the birefringence is $\Delta n_{eff} = n_e - n_0$, which can be independently determined. The value of Δn_{eff} for 5CB can be found in the literature;[18−21] and it can be found for both 5CB and 5CB/CN6 from our Freedericksz transition measurements. The measured light intensity I, obtained by analyzing images at different surfactant concentrations with the software Image-ProPlus, was used to calculate an effective birefringence, according to eq 4, thus allowing the effective birefringence versus SDS concentration curves to be constructed. We used the average intensity of the entire image, which averages over all defects in the individual grid cells and avoids any observer bias but includes both the dark grid and the bright lines due to perpendicular alignment near that grid. For this reason, Δn_{eff} will always be greater than a minimum value due to the bright lines and less than a maximum value due to the dark grid.

IV. RESULTS

The effective birefringence of the LCs, measured as a function of the surfactant concentrations, are compared for the 5CB and selected 5CB/CN6 mixtures for the three different alignment layers in Figures 7−9. In Figure 7, we compare the curves when using the PI alignment layer, at two temperatures: 24 and 30 °C.

There are several important features to be seen in Figure 7.

(a) The effective birefringence at pure water is larger for the mixture, which means (considering that the birefringence of the mixture, Δn = 0.14, is smaller than for the pure LC) that the alignment is closer to-tangential to the interface for the mixture.

(b) The decline of Δn_{eff} appears at lower concentrations of SDS when using the pure 5CB than when using the mixture.

(c) The Δn_{eff} curve for the LC mixture is less abrupt (especially at 24 °C). The more gradual the transition is, the wider is the sensing concentration range, which is an important factor for a sensor. Comparing the sensing range for the two different temperatures, we see that the sensing range increases at higher temperatures for both LCs.

(d) The effective birefringence does not drop to zero even in the homeotropic state, because the interaction of the gold frame prevents homeotropic alignment at the edges. This effect is larger for the pure 5CB, indicating that the anchoring between the gold and LC is stronger for the 5CB than for the mixture.

Figure 8 shows the same type of graphs as Figure 7, but now with OTS alignment layers beneath the LCs.

We see several notable similarities and differences with respect to the PI coating. The value of the transmitted intensity of light in the absence of SDS is ∼40% larger for the OTS coating, indicating that the OTS/LC anchoring energy is smaller than the PI/LC anchoring energy for both LCs. The sensing range is also 3−4 times wider for both LCs at 24 °C (30 °C) when using the OTS-coated surfaces, and again it is ∼40% wider for the mixture than for the pure 5CB. These almost-linear correlations between birefringence and SDS concentration make the sensors useful from 0.1 mM up to 0.9 mM for 5CB, and 0.1 mM and 1.2 mM for the 5CB/CN6 mixture.

As a final test, we used a monolayer of the bent-core Z4, prepared at a high surface pressure with the inverse Langmuir−Schaefer technique,[13] as the alignment layer. The birefringence

dx.doi.org/10.1021/am301952f | ACS Appl. Mater. Interfaces 2012, 4, 6884−6890

in the sensor using Z4 as the alignment layer, as shown in Figure 9, shows an additional 10% increase of the upper limit of

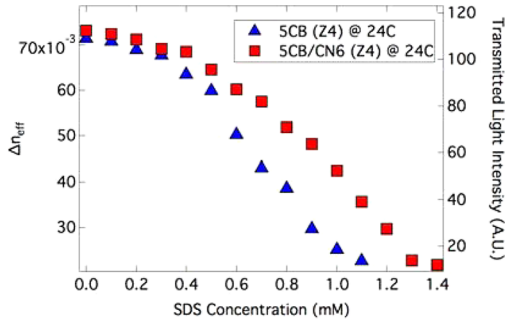

Figure 9. Birefringence and transmitted light for two different nematic liquid crystals, 5CB and the 5CB/CN6 mixture discussed in the text, versus surfactant concentration, using ILS monolayers of Z4 as the alignment layer at 24 °C.

the sensing range. This observation implies a slightly smaller anchoring strength of Z4,, compared to OTS, although they behave much more similarly to each other than to PI, because of their similar amphiphilic nature.

V. DISCUSSION

The continuous transition from the hybrid configuration to uniform homeotropic alignment has been the subject of numerous prior studies. Both the easy axis and the anchoring strength of the surface alignment at the upper water/surfactant interface may vary during the transition we report in this study. Rey, emphasizing changes in the easy axis, reported a thermodynamic model that relates the orientation of a LC to the areal density of the surfactant absorbed at the water/LC interface.[28] The Rey model has been extended to include bulk elastic distortion and estimating the surface anchoring energy as $w_0 \sin^2(\theta_s - \phi(x))$, where w_0 is assumed to be a constant, independent from the fraction of saturation monolayer coverage (x); θ_s is the tilt of LC at the interface; and ϕ is the angle of the easy axis of the LC.[6] This extension yielded a phase diagram with a two-phase region, with coexisting planar and homeotropic states of the LC. However, this region of coexistence decreased upon heating toward the isotropic phase. We, on the contrary, find an increased range of concentrations over which changes in the LC occur as a function of surfactant concentration.

In contrast to the above interpretation of the adsorbate-induced orientational transition in the LC film, resulting from a change in the easy axis of the LC, here we consider an alternative interpretation of our experiments, in terms of a change in anchoring energy. In our experiments, we find a uniform variation between the hybrid configuration and uniform homeotropic alignment, with a transitional range that increased with temperature. In addition, we find that the anchoring strength of the bottom surface influences the transition at the top surfaces as well. This latter effect has not previously been reported, and it motivated us to propose a simple model that can explain both observations by focusing on the anchoring strength, rather than the angle of the easy axis.

For our model, we need an estimate of the anchoring energy at the OTS-treated glass and Z4-monolayer-decorated interfaces. To this end, we use Barbero and Barberi's analysis,[29] which predicts that the tilt angle in the center of the film (at $z = L/2$; this is denoted as θ_{center}) is proportional to the ratios of the anchoring strengths at the opposite surfaces (see Figure 2). Moreover, θ_{center} can be calculated from the measured effective birefringence, and the ordinary and extraordinary refractive indices of the materials, as

$$\sin^2 \theta_{center} = \frac{{n_0}^2}{n_2^2 - {n_0}^2}\left[\frac{{n_e}^2}{(\Delta n_{eff} + n_0)^2} - 1\right] \quad (5)$$

Thus, values of θ_{center} can be found from Δn_{eff} measured for pure water, without SDS, for all three alignment layers with both 5CB and the 5CB/CN mixture. Furthermore, we have independent measurements of the anchoring strength at the PI/5CB and PI/(5CB/CN6) interfaces, as reported in section III.2. We can then find the anchoring strength (W_i) at the LC/alignment layer interface i from the anchoring strength W_{PI} at the LC/PI alignment layer interface and the center angles ${\theta^{PI}}_{center}$ and ${\theta^{i}}_{center}$ measured (for the same liquid crystal and upper interface) for the PI and the i alignment layers, respectively:

$$W_i = W_{PIi}\left(\frac{\theta^i_{center}}{\theta^{PIi}_{center}}\right) \quad (6)$$

The results of this calculation are shown in Table 3.

Table 3. Approximate Anchoring Energy Values for the Different Surfaces Used in This Work[a]

	Anchoring Energy (J/m^2)	
alignment layer	5CB	5CB/CN6
PI	1.4×10^{-4}	0.9×10^{-4}
OTS	0.8×10^{-4}	0.5×10^{-4}
Z4	0.7×10^{-4}	0.4×10^{-4}

[a]The values for PI are found using the method described in section III.2, while the remaining values are found from these values and θ^i_{center} (from eq 6) in the grid with the pure water upper surface, using eq 7.

Inspection of Table 3 reveals that the anchoring energies of the mixtures are smaller than those of the pure 5CB. This is probably the result of the different positions of the cyano groups in 5CB and CN6. In 5CB, it is along the molecular axis, whereas in the CN6, it is ~60° away, thus decreasing the interactions between the amphiphilic surfaces.

These anchoring energies at the bottom solid surface remain moderately strong, leading to a short extrapolation length $b_b \ll L$ (see Figure 2). The model of Barbero and Barberi[29] states that a transition from the hybrid configuration to the homeotropic alignment happens when the differences of the extrapolation lengths at the top and bottom surfaces (b_t and b_b, respectively) become larger than the film thickness L, i.e.,

$$b_t \geq L + b_b = L\left(1 + \frac{b_b}{L}\right) \quad (7)$$

In case of the observed relatively strong anchoring at the bottom, at the transition, the anchoring strength at the top interface can be approximated as

$$W_t = \frac{K}{L[1 + (b_b/L)]} \approx \frac{K}{L}\left(1 - \frac{b_b}{L}\right) \quad (8)$$

In this expression, K is the effective Frank elastic constant of the LC (K can be well-approximated with the bend elastic

dx.doi.org/10.1021/am301952f | ACS Appl. Mater. Interfaces 2012, 4, 6884−6890

constant K_3, since hybrid alignment imposes a bend in the director). Similar to Rey's model[28] for the surfactant concentration of the anchoring strength (see eq 4), near the transition, we write that

$$W_t \approx W_0\left(1 - \frac{c}{c_s}\right) \tag{9}$$

where c_s is the saturated surfactant concentration. Combining this with eq 9, the surfactant concentration c, where the transition happens, can be written as

$$c = c_s\left(1 - \frac{b_t}{L} + \frac{b_b b_t}{L^2}\right) \tag{10}$$

In accordance with our observations, the surfactant concentration at which the alignment of the LC on the top surface becomes homeotropic depends on the bend elastic constant of the LC and the anchoring strengths on both interfaces. Considering the role of the bottom interface, we see that c increases as b_b increases, i.e., with larger K and/or smaller W. Indeed, we determined experimentally that the Z4 alignment layer, which has the lowest anchoring strength, gave the largest range. Our simple model also explains the observed increase of the upper limit of the sensing range of the mixture, which has a smaller bend elastic constant (thus smaller b_t) than that of the pure 5CB.

To summarize, our results highlight the importance of the elastic and anchoring properties of the LCs used in biosensors. Specifically, we have shown that a mixture of rodlike and bent-shape molecules provide a wider sensing range with an almost-linear relationship between the surfactant concentration and the effective birefringence. Our results also suggest that the anchoring strength at the bottom surface plays a key role in the response of the LC. We found that the anchoring strength affects the sensing range, providing an improved range for the weakest anchoring. In order to qualitatively explain this improved range, and its increase with increasing temperature, we have introduced a simple model in which the switch from hybrid alignment at low surfactant concentrations to a uniform cell at high concentrations is dominated by the anchoring energy at the surfactant/liquid crystal surface. As noted above, however, both the anchoring strength and the easy axis should be functions of surfactant concentration, and both models and experiments exploring their interplay would be valuable in optimizing the range and sensitivity of the sensors.

AUTHOR INFORMATION

Corresponding Author

*E-mail: ajakli@kent.edu.

Notes

The authors declare no competing financial interest.

ACKNOWLEDGMENTS

This work was supported by NSF Grant No. DMR-0907055. The synthesis of the bent-core liquid crystal CN6 was supported by NSF No. DMR 0964765, and the material was provided by R. Brackon and R. Twieg at Kent State University. The material Z4 was provided for us by C. Tschierske at the Martin Luther University in Halle, Germany. We acknowledege technical assitance of Ms. Mir Lim in characterizing phase transitions of 5CB/CN6 mixtures. NLA acknowledges partial support from the NSF (under Award No. DMR-1121288 (MRSEC), the National Institutes of Health (Nos. CA108467 and AI092004), and by the ARO (Nos. W911-NF-11-1-0251 and W911-NF-10-1-0181).

REFERENCES

(1) de Gennes, P. G.; Prost, J. *The Physics of Liquid Crystals*, Second ed.; Clarendon Press: Oxford, U.K., 1993; Vol. *1*, pp 34−35.
(2) Cognard, J. *Mol. Cryst. Liq. Cryst.* **1982**, *51*, 1−77.
(3) Jerome, B. *Rep. Prog. Phys.* **1991**, *54*, 391−397.
(4) Brake, J. M.; Daschner, M. K.; Luk, Y.-Y.; Abbott, N. L. *Science* **2003**, *302*, 2094−2097.
(5) Brake, J. M.; Abbott, N. L. *Langmuir* **2007**, *23*, 8497−8507.
(6) Gupta, J.; Meli, M.-V.; Teren, S.; Abbott, N. L. *Phys. Rev. Lett.* **2008**, *100*, 048301-1−048301-4.
(7) Lockwood, N.; Abbott, N. L. *Curr. Opin. Colloid Interface Sci.* **2005**, *10*, 111−120.
(8) Bai, Y.; Abbott, N. L. *Langmuir* **2011**, *27*, 5719−5738.
(9) Lockwood, N.; Gupta, J.; Abbott, N. L. *Surf. Sci. Rep.* **2008**, *63*, 255−293.
(10) Frank, F. C. *Discuss. Faraday Soc.* **1958**, *25*, 19−28.
(11) Rapini, A.; Papoular, M. *J. Phys. Colloq.* **1969**, *30*, C4−54.
(12) Kardas, D.; Prehm, M.; Baumeister, U.; Pociecha, D. R.; Reddy, A.; Mehl, G. H.; Tschierske, C. *J. Mater. Chem.* **2005**, *15*, 1722−1733.
(13) Iglesias, W.; Smith, T. J.; Basnet, P. B.; Stefanovic, S. R.; Tschierske, C.; Lacks, D. J.; Jákli, A.; Mann, E. K. *Soft Matter* **2011**, *7*, 9043−9050.
(14) Brake, J. M.; Abbott, N. L. *Langmuir* **2002**, *18*, 6101−6109.
(15) Majumdar, M.; Salamon, P.; Jákli, A.; Gleeson, J. T.; Sprunt, S. *Phys. Rev. E* **2011**, *83*, 031701−1−8.
(16) Nair, G. G.; Bailey, C. A.; Taushanof, S.; Fodor-Csorba, K.; Vajda, A.; Varga, Z.; Bóta, A.; Jákli, A. *Adv. Mater.* **2008**, *20*, 3138−3142.
(17) Keith, C.; Lehmann, A.; Baumeister, U.; Prehm, M.; Tschierske, C. *Soft Matter* **2010**, *6*, 1704−1721.
(18) Tjipto-Margo, B.; Evans, G. T.; Allen, M. P.; Frenkel, D. *J. Phys. Chem.* **1992**, *96*, 3942−3948.
(19) Stewart, I. W. *The Static and Dynamic Continuum Theory of Liquid Crystals: A Mathematical Introduction*, First ed.; Taylor and Francis: New York, 2004; Vol. *1*, pp 57−132.
(20) Chen, G. P.; Takezoe, H.; Fukuda, A. *Liq. Cryst.* **1989**, *5*, 341−346.
(21) Faetti, S.; Gatti, M.; Palleschi, V. *J. Phys., Lett.* **1985**, *46*, 881−886.
(22) Breddels, P. A.; Mulkens, J. C. H. *Mol. Cryst. Liq. Cryst.* **1987**, *147*, 107−112.
(23) Bradshaw, M. J.; Raynes, E. P.; Bunning, J. D.; Faber, T. E. *J. Phys. (Paris)* **1985**, *46*, 1513−1520.
(24) Jákli, A.; Markscheffel, S.; Saupe, A. *J. Appl. Phys.* **1996**, *79*, 1891−1894.
(25) Peng, Y.; Miyamoto, T.; Naito, H.; Kuze, M.; Sugimura, A.; Iwamoto, M. *Mol. Cryst. Liq. Cryst.* **1997**, *304*, 253−258.
(26) Seo, D. S.; Kobayashi, S. *Mol. Cryst. Liq. Cryst.* **2000**, *339*, 1−10.
(27) Bechtold, I. H.; Oliveira, E. *Liq. Cryst.* **2005**, *32*, 343−347.
(28) Rey, A. D. *Langmuir* **2004**, *20*, 11473−11479.
(29) Barbero, G.; Barberi, R. *J. Phys. (Paris)* **1983**, *44*, 609−616.